Intrinsically Disordered Structure of *Bacillus pasteurii* UreG As Revealed by Steady-State and Time-Resolved Fluorescence Spectroscopy†

Paolo Neyroz,‡ Barbara Zambelli,§ and Stefano Ciurli*,§,||

Department of Biochemistry "G. Moruzzi", University of Bologna, Via San Donato 19/2, 40127 Bologna, Italy, Laboratory of Bioinorganic Chemistry, Department of Agro-Environmental Science and Technology, University of Bologna, Viale Giuseppe Fanin 40, 40127 Bologna, Italy, and CERM (Center for Magnetic Resonance), Via Luigi Sacconi 6, 50019 Sesto Fiorentino, Italy

Received February 3, 2006; Revised Manuscript Received May 11, 2006

ABSTRACT: UreG is an essential protein for the in vivo activation of urease. In a previous study, UreG from *Bacillus pasteurii* was shown to behave as an intrinsically unstructured dimeric protein. Here, intrinsic and extrinsic fluorescence experiments were performed, in the absence and presence of denaturant, to provide information about the form (fully folded, molten globule, premolten globule, or random coil) that the native state of *Bp*UreG assumes in solution. The features of the emission band of the unique tryptophan residue (W192) located on the C-terminal helix, as well as the rate of bimolecular quenching by potassium iodide, indicated that, in the native state, W192 is protected from the aqueous polar solvent, while upon addition of denaturant, a conformational change occurs that causes solvent exposure of the indole side chain. This structural change, mainly affecting the C-terminal helix, is associated with the release of static quenching, as shown by resolution of the decay-associated spectra. The exposure of protein hydrophobic sites, monitored using the fluorescent probe bis-ANS, indicated that the native dimeric state of *Bp*UreG is disordered even though it maintains a significant amount of tertiary structure. ANS fluorescence also indicated that, upon addition of a small amount of GuHCl, a transition to a molten globule state occurs, followed by formation of a pre-molten globule state at a higher denaturant concentration. The latter form is resistant to full unfolding, as also revealed by far-UV circular dichroism spectroscopy. The hydrodynamic parameters obtained by time-resolved fluorescence anisotropy at maximal denaturant concentrations (3 M GuHCl) confirmed the existence of a disordered but stable dimeric protein core. The nature of the forces holding together the two monomers of *Bp*UreG was investigated. Determination of free thiols in native or denaturant conditions, as well as light scattering experiments in the absence and presence of dithiothreitol as a reducing agent, under native or denaturing conditions, indicates that a disulfide bond, involving the unique conserved cysteine C68, is present under native conditions and maintained upon addition of denaturant. This covalent bond is therefore important for the stabilization of the dimer under native conditions. The intrinsically disordered structure of UreG is discussed with respect to the role of this protein as a chaperone in the urease assembly system.

Although the majority of enzymes need a relative rigid structure to perform their function, many proteins that have regulatory roles lack a unique tertiary structure (*1*−*3*). Native protein disorder in vivo is a way to ensure the structural malleability required for many cellular processes. This observation indicates that our traditional view of protein structure−function relationship is limited, and only partially true. Intrinsically unfolded or unstructured proteins (IUP)[1] (*4*, *5*) exist under native conditions as an ensemble of conformations, characterized by distinct and dynamic ϕ and ψ angles (*2*). In general, the function of these proteins involves binding to a partner ligand, such as another protein, a nucleic acid, a membrane, or a small molecule or metal ion. It is thought that this step induces the folding of the unstructured protein (*2*), and it is the disorder-to-order transition that allows the protein to function (*1*, *6*−*8*). In agreement with this hypothesis, recent investigations have shown that RNA and protein chaperones are the most disordered class of proteins, with 40% and 15% of predicted

† This work was supported by Grants PRIN-2001 and PRIN-2003 from the Ministero Italiano dell'Università e della Ricerca (MIUR). B.Z. was the recipient of a Ph.D. fellowship from the University of Bologna and is currently supported by a grant from University of Bologna and CERM.

* To whom correspondence should be addressed: Laboratory of Bioinorganic Chemistry, Department of Agro-Environmental Science and Technology, University of Bologna, Viale Giuseppe Fanin 40, 40127 Bologna, Italy. Phone: +39-051-209-6204. Fax: +39-051-209-6203. E-mail: stefano.ciurli@unibo.it.

‡ Department of Biochemistry "G. Moruzzi", University of Bologna.

§ Department of Agro-Environmental Science and Technology, University of Bologna.

|| CERM (Center for Magnetic Resonance).

[1] Abbreviations: bis-ANS, 4,4′-dianilino-1,1′-binaphthyl-5,5′-disulfonic acid, dipotassium salt; GuHCl, guanidine hydrochloride; DTT, dithiothreitol; DAS, decay-associated spectra; MALS, multiple-angle laser light scattering; DTNB, 5,5-dithiobis(2-nitrobenzoic acid); *Bp*, *Bacillus pasteurii*; *Ka*, *Klebsiella aerogenes*; IUP, intrinsically unfolded proteins; HSQC NMR, heteronuclear single-quantum coherence NMR spectroscopy; IRF, instrument response function; fwhm, full width at half-maximum; CD, circular dichroism.

10.1021/bi060227s CCC: $33.50
Published on Web 06/27/2006

Scheme 1

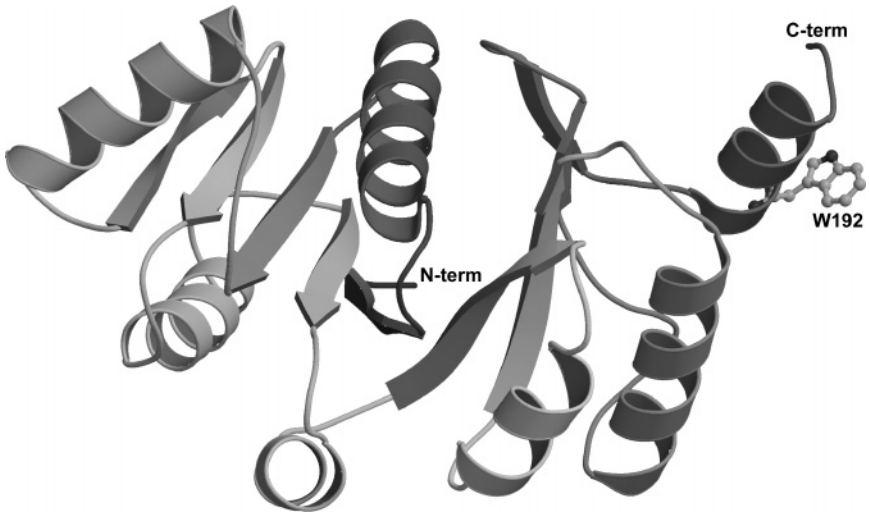

disordered regions, respectively, in segments of the polypeptide chain of ≥30 residues (*9*). The structural malleability of the region involved in binding is crucial for the different effects induced in the ligand partner when the protein undergoes the folding process (*3*, *10*). This observation is consistent with the knowledge that some proteins are able to cause opposite actions on different targets while using the same or overlapping interaction surfaces, switching the function of the interacting surface patches by adopting different conformations upon binding (*3*, *10*). The capability of the same surface to adjust to different interacting partners (binding promiscuity) can ensure very tight regulation of the formation and functioning of complexes and multicomponent systems.

When all these things are considered, it is not surprising that disorder of one or more protein chaperones involved in cellular metal trafficking and active site assembly of metalloenzymes is part of a well-designed regulatory mechanism that prevents otherwise toxic interactions of the metal ion with vital cellular components. In this respect, the trafficking of nickel and its utilization in important enzymatic systems are an example of the tight regulation mechanisms that have developed for neutralizing the extremely high toxicity of the soluble hydrated Ni^{2+} ion and for overcoming its scarcity in natural environments (*11*). Incorporation of nickel into the active site of urease, a very efficient enzyme that catalyzes urea hydrolysis (*12*, *13*), has been the subject of recent investigations driven not only by important applications for health and agriculture (*14*) but also by the peculiar, seemingly contradictory, nature of nickel as a toxic but essential metal ion. Therefore, urease can be considered a model case to improve our understanding of other analogous systems. Urease thus represents a paradigm for understanding the general principles of the mechanisms of cellular nickel trafficking.

Ureolytic organisms have evolved efficient and elaborated mechanisms of delivering the Ni^{2+} ion into its appropriate location (*15*). The mechanism of insertion of nickel into apourease is a multistep process (*16*), involving the interaction of at least four proteins, named UreD, UreF, UreG, and UreE, with the apoenzyme. We expect that structural plasticity of the individual component proteins is necessary for the assembly, in a multistep process, of the appropriate functional complex that is required for activation of the enzyme.

Of the four nickel chaperones active in the in vivo assembly of urease, only the structure of UreE, the nickel transporter (*17*−*21*), has been elucidated (*22*, *23*). Although no crystal or solution structure of the single proteins or their complexes is available yet for UreD, UreF, and UreG, several functional studies have been carried out (*24*−*31*). A complete understanding of the Ni-containing urease active site assembly implies the knowledge, at the molecular level, of the mechanisms of interaction among the metal ion, the accessory proteins, and the apoenzyme. This necessarily requires the availability of detailed information about each accessory protein structure as well as the relative biochemical properties.

The presence in the primary structure of UreG proteins of a P-loop motif, normally found to be associated with ATP or GTP binding and hydrolysis, suggests that UreG proteins are related to the in vivo GTP requirement for the assembly of the urease active site (*32*). A study of the structural features of UreG from *Bacillus pasteurii* (*Bp*UreG) was recently reported (*33*). A model of this protein in the fully folded state was obtained using threading algorithms and molecular dynamics (see Scheme 1 for a ribbon representation of the structure of *Bp*UreG). This model features an architecture typical for a GTPase protein, in agreement with the detected GTPase activity in vitro (*33*). $^{1}H-^{15}N$ HSQC NMR spectra indicated that native *Bp*UreG does not possess a rigid tertiary structure in solution but instead exists in fast equilibrium among different conformations. The same type of NMR spectrum was observed for *Ka*UreG, suggesting that this is a general feature for all UreG chaperones. In solution, *Bp*UreG exhibits a well-defined secondary structure, with both α-helices (15%) and *β*-strand regions (29%), as determined using circular dichroism (CD) spectroscopy. The comparison between the amount of secondary structure estimated from CD measurements and that derived from the molecular model of *Bp*UreG indicated that the purified protein contains an amount of α-helices smaller than that predicted by the computational studies. It was suggested that the contradiction between the theoretically predicted and the experimentally determined secondary structure could involve mostly the more solvent-exposed α-helices rather than the

β-strands, and that the internal β-barrel is maintained (*33*). It was suggested that UreG proteins belong to the family of intrinsically unstructured proteins, possibly requiring the interaction with other partner chaperones in assuming the completely folded, functional form (*33*). This hypothesis was consistent with previous studies that demonstrated that *Ka*UreG is able to form a *Ka*UreDFG complex in vivo (*34*).

In an effort to obtain experimental data that would clarify the molecular characteristics of the UreG protein, and in particular to elucidate the folded state of the protein, we undertook a study of the structural properties of *Bp*UreG in solution using fluorescence spectroscopy, performed both in the steady state and in the time-resolved mode. Two different aspects make this approach interesting and significant. First, *Bp*UreG contains a unique tryptophan residue (W192), located in the α-helical C-terminal region that could not be modeled due to the lack of a structural template for this segment (*33*) (see Scheme 1). Therefore, the strong intrinsic fluorescence of W192 offers the possibility of gaining structural information about the C-terminal region of the protein. Second, the intrinsic fluorescence of W192 as well as that of bis-ANS, a probe used to study the solvent-exposed hydrophobic patches of proteins, was monitored in the presence of increasing amounts of a denaturing agent in an effort to characterize the local and global folding properties of the native protein. The results of this study allowed us to better comprehend the unusual structural properties of *Bp*UreG, a protein that operates in solution as a stable folding intermediate depending upon ligand binding or protein−protein interaction to achieve a folded state.

EXPERIMENTAL PROCEDURES

Materials. Guanidine hydrochloride (GuHCl), melatonin, Ellman's reagent, 5,5-dithiobis(2-nitrobenzoic acid) (DTNB), and all buffer salts were from Sigma-Aldrich Co. (St. Louis, MO). Bis-ANS (4,4′-dianilino-1,1′-binaphthyl-5,5′-disulfonic acid, dipotassium salt) was purchased from Molecular Probes (Eugene, OR). Purification of recombinant *Bp*UreG was performed as reported previously (*33*). The purified protein under native conditions was shown to be exclusively a dimer of 46 kDa as confirmed by light scattering measurements (*33*).

Fluorescence Measurements and Data Analysis. Steady-state fluorescence intensities and emission spectra were recorded using a PTI QuantaMaster C60/2000 (Photon Technology International, Inc.) spectrofluorometer, operating in "photon counting" mode. Excitation and emission bandpasses were set to 2.5 nm each. An excitation wavelength of 295 nm was used, unless differently stated. Absorbance at the excitation wavelength of 295 nm was always below 0.15.

Fluorescence quenching measurements of the *Bp*UreG protein were performed using potassium iodide (KI) as a quencher. Protein samples containing increasing concentrations of the quencher were prepared by adding small aliquots from a concentrated solution of KI (4 M). KI stock solutions were freshly prepared in the presence of 1×10^{-4} M $Na_2S_2O_3$ to avoid I_3^- formation (*35*). Emission spectra, recorded as a function of the quencher concentration, were corrected for the Raman contribution of the solvent buffer and then integrated using Felix 1.42 (Photon Technology International, Inc.). These steady-state fluorescence data were then analyzed according to the general form of the Stern−Volmer equation for collisional quenching (*35*, *36*):

$$\frac{F_0}{F} = 1 + K_{SV}[Q] \quad (1)$$

where F_0 and F are the fluorescence intensities measured in the absence and the presence of the quencher, respectively, K_{SV} is the Stern−Volmer constant, and [Q] is the quencher concentration. Moreover, K_{SV} is equal to $k_q\tau_m$, where k_q is the apparent second-order rate constant for the collisional quenching process that represents a measure of the overall solvent accessibility of the fluorophores and τ_m is the intensity-weighted mean fluorescence lifetime (*37*).

Steady-state anisotropy measurements were performed using the same instrument with automated rotating Glan-Thompson polarizers placed in the excitation and emission path. The intensities of the parallel (vv) and the perpendicular (vh) components of the polarized fluorescence emission were then used to obtain the steady-state anisotropy, $\langle r \rangle$, as follows:

$$\langle r \rangle = \frac{I_{vv}G - I_{vh}}{I_{vv}G + 2I_{vh}} \quad (2)$$

where G, the "grating" correction factor, was equal to I_{hh}/I_{hv}.

For the experiments in the presence of bis-ANS, different concentrations of GuHCl were added to a 50 mM Tris-HCl solution (pH 7.5) at 22 °C containing 0.7 mg/mL *Bp*UreG and 0.5 mM bis-ANS, and after a 10 min period of incubation, fluorescence spectra of bis-ANS were recorded using an excitation wavelength of 375 nm.

Nanosecond time-resolved fluorescence measurements were taken by the time-correlated single-photon counting method (*36*), using a model 5000U fluorescence lifetime spectrometer (IBH Consultants Ltd., Glasgow, U.K.) equipped with a Thyratron gated spark lamp. A computer-controlled rotating sample holder was used to collect multiple emission wavelength decay curves or the parallel and perpendicular components of the fluorescence intensity decay. The following instrumental settings were then used to obtain the decay-associated spectra (DAS) and anisotropy decay data (see below). The instrument response function (IRF) was typically 1.4 ns (fwhm) using a Hamamatzu R3235 photomultiplier; with reconvolution methods, it is theoretically possible to resolve lifetime components that are 10% of the fwhm, which here is approximately 0.14 ns. The data were collected into 1024 channels at a timing resolution of 0.103 ns/channel. Melatonin was used as a reference standard for pure monoexponential decay, and under these experimental conditions, the estimated resolution was typically 0.2−0.3 ns. Typical reconvolution procedures were utilized to treat the experimental fluorescence decay data (*38*), and the resulting data were analyzed by the nonlinear least-squares method assuming the fluorescence intensity decay as a sum of discrete exponential components, each described by a decay constant (lifetime, τ_i, in nanoseconds) and its relative contribution (amplitude, α_i) to the total fluorescence decay (*38*):

$$I(t) = \sum \alpha_i e^{-t/\tau_i} \quad (3)$$

The decay constants were accurately determined by collecting the fluorescence (10 000 counts at the peak maximum) at four different emission wavelengths (330, 335, 340, and 345 nm) and analyzing the experimental data (all the channels with counts > 0.5% of the counts in the peak over the first 512 channels of the total decay) using the global procedure, linking common lifetimes (i.e., each decay curve will be described by identical decay constants but different corresponding amplitudes, as described above) (*39*). The DAS were obtained by collecting fluorescence decay curves at multiple emission wavelengths, from 304 to 400 nm in steps of 2 nm (*39*). All available data were simultaneously analyzed using the linked and fixed lifetimes, determined as described above, using the global procedure.

The decay of the emission anisotropy of *Bp*UreG was measured as previously described (*40*). Vertical polarized excitation was obtained using a Glan-Thompson polarizer placed on the excitation path, whereas emission was analyzed using a combination of two Polacoat dichroic polarizers oriented parallel (vv) and perpendicular (vh) with respect to the excitation polarization. A DPU-15 depolarizer (Optics for Research) placed in front of the emission monochromator slit was used to minimize *G*-factor corrections ($G = 1.007$). Decay curves of the polarized components of the emitted fluorescence were separately collected within the same experimental time course by alternative collection of the "I_{vv}" and "I_{vh}" curves, plus the exciting function, or IRF, which was determined using a solution of colloidal silica.

Fluorescence anisotropy decay data were analyzed assuming an exponential function of the following form:

$$r(t) = \sum \beta_i e^{-t/\phi_i} \tag{4}$$

where β and ϕ represent the anisotropy observed in the absence of rotation, r_0, and the rotational correlation time (nanoseconds) associated with the molecule motion, respectively. According to this view, the transients of the polarized emission components, $I_{vv}(t)$ and $I_{vh}(t)$, were fitted to obtain $r(t)$ as (*41*)

$$I_{vv}(t) = \frac{1}{3}s(t)[1 + 2r(t)] \tag{5}$$

$$I_{vh}(t) = \frac{1}{3}s(t)[1 + r(t)] \tag{6}$$

where $s(t)$ represents the decay of the total emitted fluorescence. For a globular protein that approximates the spherical symmetry, the anisotropy decay is reduced to a single exponential.

Under these conditions, the correlation time can be related to the hydrated volume of the rotating protein, *V*, by the Einstein−Stokes relation; $\phi = V\eta/kT$, where η is the solvent viscosity, *k* is the Boltzmann constant, and *T* is the experimental temperature. Typically, deviations of the complex anisotropy decays, or correlation times, of ≥12% of the value predicted by the molecular weight calculations suggest divergence from simple spherical symmetry (i.e., prolate ellipsoid shape of the protein) (*36*).

The quality of the fit statistics was judged by the plot of the weighted residuals, the autocorrelation function of the residuals, and the value of the reduced χ^2 (*42*). Errors associated with the recovered decay parameters (at the 67% confidence level) were calculated using rigorous error analysis as described elsewhere (*41*). Unless otherwise stated, all the fluorescence experiments were carried out at 24 °C in 50 mM Tris-HCl buffer at pH 8.0.

Equilibrium Unfolding Measurements and Data Analysis. To monitor the unfolding conformational transition of *Bp*UreG as a function of GuHCl concentration, small aliquots (25−1500 μL) of denaturant from a 6 M stock solution were added by microsyringe to a protein sample (0.7 mg/mL) with an initial volume of 2 mL. The samples were equilibrated at 24 °C before the entire emission spectrum was recorded. The observed spectral features did not change after an incubation time of 10 min and were found to be constant even after 48 h in a manner independent of the denaturant concentration. Data were corrected for dilution as $F_{cor} = F_{obs}(V_t/V_i)$, where F_{cor} and F_{obs} indicate the dilution-corrected and observed fluorescence intensities, respectively, V_i represents the initial sample volume in the absence of denaturant, and V_t is the total sample volume after the addition of denaturant.

To describe a two-state transition, N ⇌ U, between the native and unfolded states with an unfolding equilibrium constant ($K_{un} = [U]/[N]$) and a free energy change given by

$$\Delta G^\circ_{un} = -RT \ln K_{un} \tag{7}$$

the following linear relationship (linear extrapolation model) was used to describe the thermodynamics of the denaturant-induced unfolding of proteins (*43*, *44*):

$$\Delta G^\circ_{un} = \Delta G^\circ_{0,un} - m[D] \tag{8}$$

where $\Delta G^\circ_{0,un}$ is the free energy change of unfolding extrapolated to zero denaturant concentration at a reference temperature and *m*, the denaturant concentration index, is a measure of the dependence of ΔG°_{un} on denaturant concentration. Equilibrium denaturation data analysis was performed as previously described (*44*). The following equation was used to fit the experimental data by a two-state transition model (*44*):

$$X = \frac{X_{0N} + S_N[D] + (X_{0U} + S_U[D]) \cdot e^{\frac{-\Delta G^0_{0,un} + m[D]}{RT}}}{1 + e^{\frac{-\Delta G^0_{0,un} + m[D]}{RT}}} \tag{9}$$

where X_{0N} and X_{0U} indicate either the fluorescence intensities, the wavelength λ_{max}, or the steady-state anisotropy ($\langle r \rangle$) of the native and unfolded states in the absence of the denaturant, respectively, and the terms S_N and S_U represent the baseline slopes for the native and unfolded regions, respectively. In our analyses, we refer to the exhaustive survey by Eftink (*44*) on the use of fluorescence methods to monitor unfolding transitions in proteins. According to that study, the slope ($s_i = dS_i/d[D]$) describes the trend of the change of the spectroscopic parameter S_i versus [D]; these terms add two fitting parameters in the analysis. In this work, when λ_{max} and $\langle r \rangle$ data were analyzed according to eq 9 with free-floating S_N and S_U parameters, fitting functions that properly traced the transition were obtained, but large errors affected the parameters, likely indicating the existence of nonunique solutions. In particular, the procedure systematically failed to recover the appropriate initial and final λ_{max}. This result occurred regardless of the calculated baseline slopes, which were very closely proximate to zero (S_N =

0.002, $S_U = 0.0006$). Thus, because these baseline slope terms tend to zero whether λ_{max} or $\langle r \rangle$ values are used, these parameters were fixed to zero in the analysis procedure. When these constraints were imposed, the initial and final recovered spectroscopic parameters were very close to the experimental data and reasonable error estimates were obtained. Equation fitting was carried out using the nonlinear least-squares utility included in SigmaPlot 8.0 (SPSS Science Software).

Light Scattering Experiments. Absolute estimates of the molecular mass of *Bp*UreG under native conditions or in 3 M GuHCl in the absence or presence of dithiothreitol (DTT) were determined using a combination of size exclusion chromatography and multiple-angle light scattering (MALS). In the absence of DTT, *Bp*UreG (100 μL, 2.5 mg/mL) in 50 mM Tris-HCl buffer (pH 8.0), 200 mM NaCl, containing 3.0 M GuHCl, was loaded onto an S-75 HR10/30 column (Amersham) pre-equilibrated with the same buffer and eluted at 25 °C at a flow rate of 0.5 mL/min. Another sample was incubated for 10 min in the same buffer that is described above but also containing 2 mM DTT and then eluted in the same buffer, as described above. Analogous conditions were used for native *Bp*UreG in the presence of 2 mM DTT. The column was connected downstream to a multiangle laser light (690.0 nm) scattering DAWN EOS photometer (Wyatt Technology). The concentration of the eluted protein was determined using a refractive index detector (Optilab DSP, Wyatt). Values of 0.185 for the refractive index increment (d*n*/d*c*) and 1.323 or 1.369 for the solvent refractive index in the absence or presence of 2 mM DTT, respectively, were used. Molecular weights were determined from a Zimm plot. Data were analyzed using Astra 5.1.7 (Wyatt Technology), following the manufacturer's indications.

Determination of the Amount of Free Cysteine Thiols in BpUreG. Purified *Bp*UreG (0.4 mL, 4 mg/mL) was dissolved in 0.96 mL of 20 mM Tris-HCl buffer (pH 8.0) containing 150 mM NaCl. An identical sample was prepared, which additionally contained 3.0 M GuHCl. A solution of DTNB (40 μL, 10 mM) was added to each sample, and the reaction mixtures were incubated at room temperature overnight. The absorbance at 412 nm was measured. The values obtained for *Bp*UreG, with or without guanidinium chloride, were compared to standard cysteine concentrations under identical conditions of concentration and buffer.

Circular Dichroism Spectroscopy. CD spectra of *Bp*UreG in 50 mM Tris-HCl buffer (pH 8.0) and 200 mM NaCl, in the presence of increasing amounts of GuHCl, were measured at 25 °C, using a JASCO 810 spectropolarimeter flushed with N_2, and a cuvette with a 0.1 cm path length. The near-UV and far-UV CD spectra were registered at 0.2 nm intervals in the wavelength ranges of 270−340 and 200−240 nm, using 500 μL samples of 2.5 and 0.23 mg/mL *Bp*UreG, respectively. Ten spectra were accumulated at room temperature and averaged to achieve an appropriate signal-to-noise ratio. The spectrum of the buffer was subtracted.

RESULTS

Steady-State Intrinsic Fluorescence Spectroscopy. *Bp*UreG contains one tryptophan residue (W192) and four tyrosine residues (Y31, Y41, Y120, and Y154). The steady-state excitation and emission spectra of the intrinsic fluorescence of *Bp*UreG recorded under native conditions are presented in Figure 1 together with the emission spectrum obtained in the presence of 3.0 M guanidine.

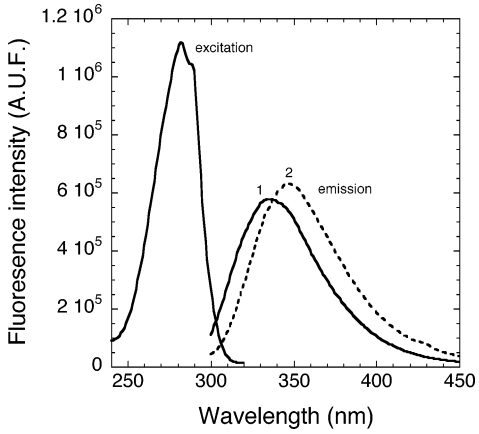

FIGURE 1: Steady-state excitation and emission spectra of *Bp*UreG. Excitation and emission spectra were recorded using a band-pass of 2.0 nm on each side. For the excitation spectrum, the emission was selected at 335 nm, and for the emission spectra, an excitation wavelength of 295 nm was used. The native protein (0.4 mg/mL) was dissolved in 50 mM Tris-HCl (pH 8.0) at 24 °C. The solid line spectra were recorded in the absence of GuHCl, whereas the dashed line emission spectrum was recorded in the presence of 3.0 M GuHCl.

Under native conditions, emission spectra were obtained by exciting the protein in both the tryptophan, 295 nm (Figure 1, curve 1), and tyrosine, 275 nm, absorption bands. No differences in the steady-state emission spectral profiles were observed, suggesting that the tryptophan residue emission dominates the intrinsic fluorescence of *Bp*UreG.

Under native conditions, the maximum of the fluorescence intensity was centered at 336 nm, as expected for chromophores buried inside the protein. On the other hand, in the presence of 3.0 M guanidine hydrochloride (GuHCl) denaturing agent (Figure 1, curve 2), the emission spectrum of *Bp*UreG was shifted to 347 nm and its intensity increased approximately 10%, suggesting a conformational change that exposes W192 to the solvent.

To further characterize the changes in the tryptophan residue accessibility induced by the denaturing agent, measurements of fluorescence quenching induced on *Bp*UreG by the addition of potassium iodide (KI) were performed under native (N) and denaturing (U) conditions (3.0 M GuHCl). The Stern−Volmer constants [$K_{SV}(N) = 1.2\ M^{-1}$ and $K_{SV}(U) = 3.9\ M^{-1}$] were recovered from a fit to the points shown in Figure 2A. The good linearity of the plots indicates that the quenching process is purely collisional under both conditions. The bimolecular quenching rates [$k_q(N) = 0.35 \times 10^9\ M^{-1}\ s^{-1}$ and $k_q(U) = 1.19 \times 10^9\ M^{-1}\ s^{-1}$] were calculated using the intensity-weighted mean lifetimes ($\tau_{mN} = 3.43$ ns and $\tau_{mU} = 3.28$ ns) for *Bp*UreG in the native and denatured state, respectively (see the footnotes of Table 2). The observed changes in the quenching, K_{SV}, and diffusional, k_q, parameters, coupled with the reported change of the position of the maximum in the emission spectra, clearly indicate that the tryptophan residue moves from a hydrophobic-buried to a more polar-exposed environment upon addition of GuHCl.

This conclusion was further supported by the analysis of the near-UV circular dichroism spectra of *Bp*UreG under

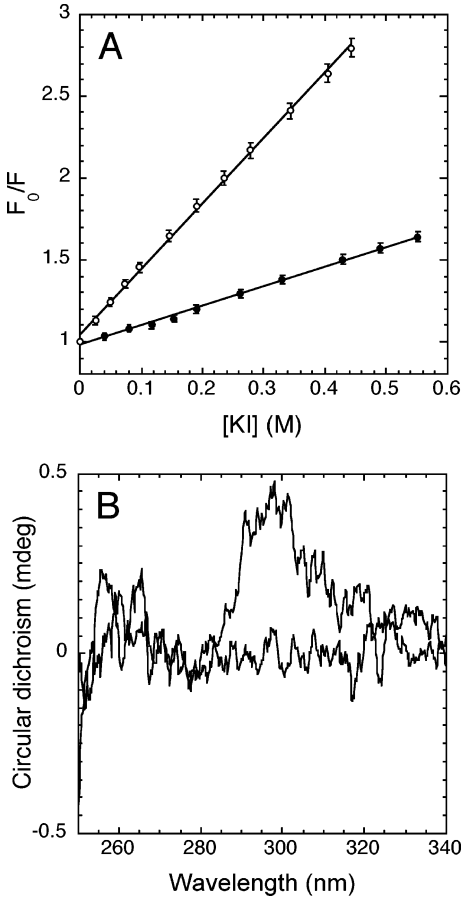

FIGURE 2: Spectroscopic evaluation of the tertiary structure of *Bp*UreG. (A) Stern−Volmer plots of the intrinsic fluorescence of *Bp*UreG. Steady-state fluorescence intensity measurements were performed at 24 °C using an excitation wavelength of 295 nm and observing the emission at 335 and 347 nm, with the protein in the absence (●) and presence (○) of 1.2 M GuHCl. The protein samples (15 μM) were dissolved in a buffer containing 50 mM Tris-HCl at pH 8.0, and small aliquots of KI (4 M) were added by microsyringe. The straight lines correspond to the linear regression analyses of the data fitted according to eq 1; the recovered K_{SV} values were 1.1997 and 3.896 M^{-1} for the experiments carried out in the absence and presence of GuHCl, respectively. (B) Near-UV CD spectra of *Bp*UreG in the absence (thick line) and presence (thin line) of 3 M GuHCl.

Table 1: Thermodynamics of the Equilibrium Unfolding Conformational Transition of the *Bp*UreG Protein[a]

	$\Delta G^\circ_{0,un}$	m	C_m (M)
λ_{max}	1.47 ± 0.54	1.58 ± 0.42	0.93 ± 0.11
$\langle r \rangle$	1.77 ± 0.23	1.57 ± 0.18	1.13 ± 0.07

[a] $\Delta G^\circ_{0,un}$ (kilocalories per mole), the free energy change of unfolding extrapolated to zero GuHCl concentration, and m (kilocalories per mole per molar), the dependence of $\Delta G^\circ_{0,un}$ on denaturant concentration, were obtained from the nonlinear least-squares fitting of the data presented in Figure 3B. C_m is the GuHCl concentration at half-denaturation, obtained as $\Delta G^\circ_{0,un}/m$. The errors in $\Delta G^\circ_{0,un}$ and m were recovered from the nonlinear least-squares analysis, while those in C_m were obtained from the relative propagation of errors (*42*).

native conditions and in the presence of 3 M GuHCl. The CD spectrum in the 250−350 nm wavelength region can be sensitive to certain aspects of protein tertiary structure. At these wavelengths, the chromophores are the aromatic amino acids, and the CD signals that they produce are sensitive to the overall tertiary structure of the protein. Signals in the region from 250 to 270 nm can be attributed to phenylalanine residues; signals from 270 to 290 nm are referred to tyrosine, and those from 280 to 300 nm can be assigned to tryptophan (*45*). In the spectrum of the native protein, a band covering the 280−300 nm range is clearly visible, indicating the presence of local tertiary structure around the unique W192 (Figure 2B), and the band disappears in 3 M GuHCl.

Table 2: Time-Resolved Fluorescence Intensity Decay Parameters

protein state[a]	α_1	τ_1 (ns)[b]	α_2	τ_2 (ns)	α_3	τ_3 (ns)	χ^2
N	0.84[c]	0.58[c]	0.65[c]	2.17[c]	0.27[c]	5.56[c]	1.24[c]
U	0.86[c]	0.35[c]	0.77[c]	2.05[c]	0.24[c]	5.45[c]	1.15[c]

[a] N (native) and U (unfolded) indicate the protein state and the time-resolved parameters obtained with the protein in the absence and presence of denaturant (3 M GuHCl), respectively. Experiments were carried out in 50 mM Tris-HCl (pH 8.0) at 24 °C. To accurately measure the intrinsic fluorescence decay of *Bp*UreG, the excitation wavelength was 295 nm and fluorescence decay curves were collected at 330, 335, 340, and 345 nm with linking common lifetimes in each decay curve. The data presented refer to the emission decay recorded at 335 nm. The decay constants reported in the table were used as fixed common parameters to obtain the DAS depicted in Figure 7. Band-passes of 32 and 16 nm were used in the excitation and emission path, respectively. [b] The intensity decay curves were best fitted by three discrete exponential decay components. With τ_i values are indicated the decay constants and with α_i values their relative amplitudes. From these data, the intensity-weighted mean lifetimes ($\tau_{mN} = 3.43$ ns and $\tau_{mU} = 3.28$ ns) were calculated: $\tau_{mj} = \sum(\alpha_i\tau_i^2)/\sum(\alpha_i\tau_i)$. [c] Errors of the recovered parameters were estimated as the lower and upper bound of the joint confidence interval calculated for a 67% probability level and never exceeded 10% of the reported values (e.g., $\alpha_1 = 0.79 < 0.84 < 0.90$, $\tau_1 = 0.52 < 0.58 < 0.65$ ns, $\alpha_2 = 0.58 < 0.65 < 0.72$, $\tau_2 = 1.94 < 2.17 < 2.41$ ns, $\alpha_3 = 0.23 < 0.27 < 0.31$, and $\tau_3 = 5.31 < 5.56 < 5.82$ ns).

The local conformational transitions affecting the tryptophan peptide chain of *Bp*UreG were monitored by following the changes in the protein intrinsic fluorescence spectra previously observed (Figure 1) as a function of increasing GuHCl concentration (Figure 3A). The observed modest increase in fluorescence intensity did not provide sufficient information to precisely trace a conformational modification. On the other hand, the changes in the emission maxima (λ_{max}) as a function of GuHCl concentration had a clear sigmoidal profile (Figure 3B), thus revealing a transition between two states, each possessing distinct spectroscopic properties. To better define the nature of the observed photophysical transition and to relate this change to molecular structural parameters, we performed measurements of the steady-state fluorescence anisotropy, $\langle r \rangle$, as a function of denaturant concentration. Fluorescence anisotropy can be used to directly monitor the rotational dynamics of molecules in solution. Changes in $\langle r \rangle$ are used to probe overall changes in the hydrated volume of proteins (for example, as a consequence of protein oligomerization or protein unfolding) as well as changes in the segmental motions of peptide chains (for example, by increasing the mobility of a protein portion). Panel B of Figure 3 shows that the transition curves obtained using changes in λ_{max} and $\langle r \rangle$ can be consistently described by a two-state model: W192−peptide chain in the native state versus W192−peptide chain in the unfolded state, with a GuHCl concentration at half-denaturation (C_m) of ca. 1 M. The results of the two-state fitting analysis of these curves are reported in Table 1. The free energy of unfolding obtained by monitoring λ_{max} and $\langle r \rangle$ are very similar ($\Delta G^\circ_{0,un} = 1.47 \pm 0.54$ kcal/mol and $\Delta G^\circ_{0,un} = 1.77 \pm 0.23$ kcal/mol, respectively). As described in Experimental Procedures, these

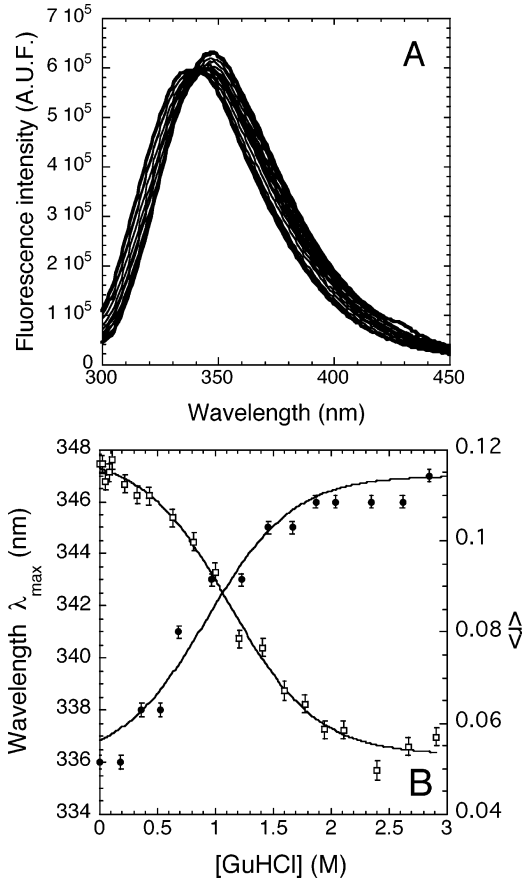

FIGURE 3: Conformational transition of *Bp*UreG as revealed by steady-state fluorescence signals. (A) Steady-state emission spectra of *Bp*UreG (0.7 mg/mL) in 50 mM Tris-HCl (pH 8.0) at 24 °C at increasing concentrations of GuHCl (from 0 to 3 M, incubation time of 10 min). The excitation wavelength was 295 nm, and the band-pass was 2.5 nm on both the excitation and the emission side. (B) Changes in λ_{max} (●) and steady-state anisotropy (□) as a function of denaturant concentration. The solid lines represent the fits by a nonlinear least-squares method of the experimental data. A two-state model of the form reported in eq 9 was used, and the results are reported in Table 1.

results were obtained by fixing the baseline slope terms to zero to provide reasonable convergence in the data analysis. When free-floating slope terms were used, this choice negatively affected the recovery of the searched parameters and the relative error estimates. These analysis penalties were mainly observed with the λ_{max} data, whereas the steady-state anisotropy data provided values of 0.005 and 0.004 for S_N and S_U, respectively, with a recovered $\Delta G°_{0,un}$ of 1.93 ± 1.16 kcal/mol (m = 1.49 ± 0.72 kcal mol^{-1} M^{-1}), which did not substantially differ from the value reported in Table 1, obtained with fixed null S_N and S_U values.

Moreover, the transitions reported in Figure 3B appear to occur with an identical denaturant concentration index (m = 1.58 ± 0.42 kcal mol^{-1} M^{-1} and m = 1.57 ± 0.18 kcal mol^{-1} M^{-1}), suggesting that the two different methods are tracing the same conformational transition, yet the low values measured for the index m indicate a scarcely cooperative process. Intrinsic fluorescence measurements of proteins simply probe the environment of tryptophan residues. In *Bp*UreG, W192 is part of the C-terminal helical peptide chain (see Scheme 1), and the low thermodynamic parameters found ($\Delta G°_{0,un} \approx$ 1.5 kcal/mol) are consistent with a small

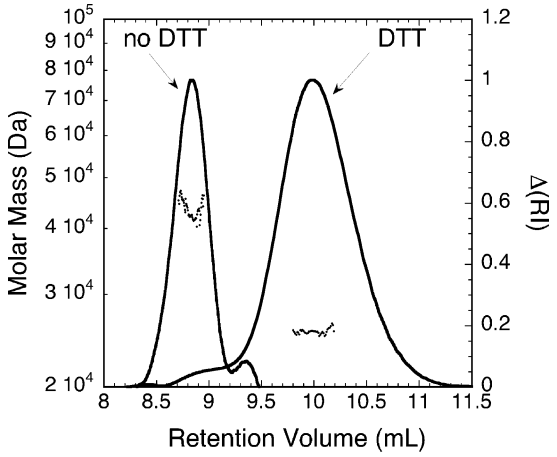

FIGURE 4: Molar mass distribution plot for *Bp*UreG under denaturing conditions. Elution profile of *Bp*UreG in 3 M GuHCl in the absence and presence of 2 mM DTT. The solid line indicates the trace from the refractive index detector, and the dots are the weight-average molecular weights for each slice (measured every second) as calculated from the multiple-angle light scattering data. The other experimental conditions are described in the text.

molecular rearrangement rather then a global unfolding process (typically characterized by $\Delta G°_{0,un} > 4.0$ kcal/mol). Moreover, the residual steady-state anisotropy at the maximal denaturant concentration ($\langle r \rangle \approx 0.05$ at 3 M GuHCl) suggests the existence of significant hindrance to a high level of rotational freedom as expected for completely unfolded proteins ($\langle r \rangle \approx 0.005$), supporting the fact that at 3.0 M GuHCl the protein is still partially folded. As suggested by several studies (*46*−*48*), a possible interpretation of these results is that they are related to the process of rupture of the dimer of *Bp*UreG, known to be the largely predominant form present in solution (*33*), into the corresponding monomers. However, this possibility was excluded on the basis of multiple-angle light scattering (MALS) experiments conducted in the presence of 3 M GuHCl (*49*, *50*) (Figure 4), which are consistent with the presence of the dimeric form of the protein (calculated molar mass of 46.4 ± 0.5 kDa). To elucidate the nature of the interactions determining the dimeric state of *Bp*UreG, we investigated the possible role of the fully conserved (*33*) single cysteine residue (C68 in *Bp*UreG). No free thiol was found in the absence or presence of 3 M GuHCl, using Ellman's reagent (*51*), as evidenced by negligible absorbance at 412 nm as compared to a standard cysteine solution. This evidence suggests that a disulfide bond is present under native conditions and is maintained upon addition of denaturant, thereby explaining the unusual stability of the dimer. This was confirmed by MALS experiments conducted on *Bp*UreG under denaturing conditions in the presence of 2 mM DTT, which revealed the dissociation of the dimer into the corresponding monomer subunits (Figure 4). The presence of a disulfide bond in purified *Bp*UreG is not surprising if one considers that the last steps of the isolation procedure are carried out in air and in the absence of reducing agents, conditions that may favor disulfide bond formation if the cysteine residues are close in space in a preformed dimer. The latter was indeed shown to exist in MALS experiments conducted under native conditions in the presence of DTT. The physiological role of the disulfide bond found in the *Bp*UreG dimer has yet to be demonstrated.

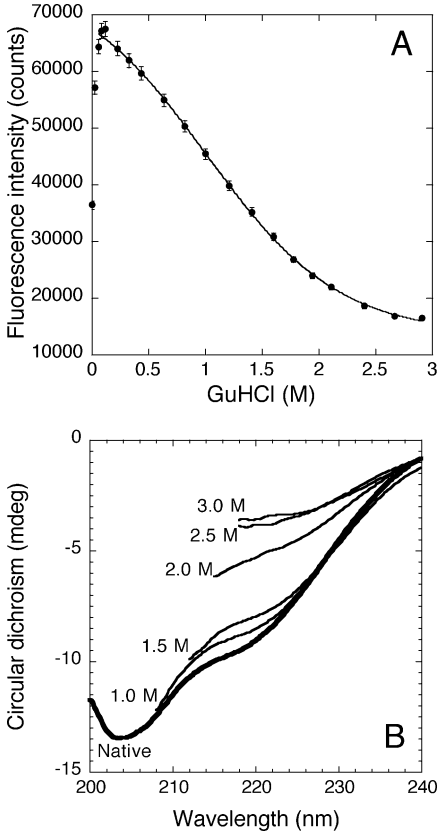

FIGURE 5: Equilibrium denaturation by GuHCl of the *Bp*UreG monitored by bis-ANS fluorescence and CD spectroscopy. (A) Plot of the ANS fluorescence of *Bp*UreG as a function of GuHCl concentration. To a sample solution containing *Bp*UreG (0.7 mg/mL) in 50 mM Tris-HCl (pH 7.5) was added bis-ANS at a final concentration of 0.5 mM, at 24 °C. Different concentrations of GuHCl were added, and after a 10 min period of incubation, fluorescence spectra of bis-ANS were recorded using an excitation wavelength of 375 nm and reading the fluorescence intensity at 516 nm, with a band-pass of 2 nm on each side. In the graph, the solid line through the symbols represents the fitting of the data to a two-state model in the 0.06−0.3 M GuHCl concentration range. (B) Far-UV CD spectra of *Bp*UreG as a function of GuHCl concentration. The spectrum in the native state is shown with a thick line. The concentration of denaturant for each spectrum is indicated.

To extend the analysis of the effect of denaturant from the local tryptophan environment to the overall protein structural architecture, the binding of bis-ANS to the protein was analyzed as a function of increasing concentrations of GuHCl. This fluorescent probe binds to hydrophobic, nonpolar surfaces of proteins with high affinity and exhibits a significant fluorescence enhancement upon binding (*52*, *53*). The data obtained with *Bp*UreG are presented in Figure 5A. The initial fluorescence intensity, obtained in the absence of GuHCl, is noticeably higher than that expected for a fully folded protein, with a maximum emission wavelength at 516 nm that did not change with an increase in the GuHCl concentration. These findings are consistent with the presence of a significant number of exposed hydrophobic sites under native conditions. Figure 5A further shows that a 2-fold increase in the fluorescence intensity of bis-ANS occurs at very low denaturant concentrations, with a strong peak at 0.1 M GuHCl, indicative of the formation of a more unfolded intermediate, characterized by the maximal exposure of the protein hydrophobic core (*54*, *55*). The peak is followed by a slow decrease in the fluorescence upon addition of GuHCl up to 3.0 M, which may well be related to the gradual disruption of the residual hydrophobic patches eventually leading to the fully unfolded form of the protein. The bis-ANS data were analyzed by a two-state transition model in the 0.06−3.0 M GuHCl concentration range (solid line in Figure 5). The recovered thermodynamic parameters ($\Delta G^{\circ}_{0,un} = 1.01 \pm 0.11$ kcal/mol; $m = 1.00 \pm 0.08$ kcal mol^{-1} M^{-1}) are as low as the parameters measured for the local conformational transition monitored using the steady-state W192 fluorescence anisotropy and the λ_{max} denaturation curves (Table 1). This observation suggests that both the local and global unfolding transitions detected are phenomena that have essentially a similar nature and that involve the rupture of weak interactions without dramatic modifications of the protein architecture.

The effect of denaturant on the secondary structure of *Bp*UreG was studied by far-UV CD spectroscopy. On the basis of the ellipticity at 222 and 218 nm of the spectra shown in Figure 5B, it can be inferred that no dramatic modifications of the α-helix and β-sheet composition of the protein structure were observed up to 1.5 M GuHCl. On the other hand, a significant reduction in the level of these structural elements occurs above this denaturant concentration. Moreover, at the limit of 3 M GuHCl, the persistence of negative ellipticity in the observed wavelength range, in contrast to the expected positive ellipticity typical for a protein in the random coil conformation, indicates that the protein still retains some secondary structure.

Time-Resolved Intrinsic Fluorescence Spectroscopy. Resolution of the dynamics underlying the steady-state fluorescence data generally provides useful information that relates the protein photophysical parameters to the structural properties of the molecule. Here, the intrinsic emission decay of *Bp*UreG was studied in the nanosecond time domain. Measurements were performed by the time-correlated single-photon counting method with excitation at 295 nm and observation of the emission either at a single wavelength or at multiple wavelengths. Simultaneous analysis of decay curves collected across the emission spectra was then used to resolve the DAS. A typical fluorescence intensity experimental decay is shown in Figure 6. The plot of the autocorrelation function of the weighted residuals, used to judge the quality of the fitting, is also presented in Figure 6. The results of the analysis of the data obtained at the emission wavelength of 335 nm with *Bp*UreG in the absence and presence of 3.0 M GuHCl are reported in Table 2. The intrinsic fluorescence decay of *Bp*UreG in the native state was adequately described by three discrete decay components ($\tau_1 < 0.6$ ns, $\tau_2 = 2.1$ ns, and $\tau_3 = 5.5$ ns), as typically found even for proteins containing a single tryptophan residue. With the exception of the change in the shortest lifetime (at the limit of our instrumental time resolution), which accounts for 4−5% of the total emission intensity, no significant differences in the lifetimes were observed in the presence of the denaturant. On the contrary, under this condition, the relative amplitude, α_2, associated with τ_2 revealed a significant increase. This distinct effect could be better evaluated by the resolved DAS depicted in Figure 7. It is shown that, in the native state, the spectra associated with $\tau_1-\tau_3$ were centered at 310, 330, and 340 nm, respectively. Under this condition, the integrated areas under DAS_1, DAS_2, and DAS_3 provided a relative contribution of

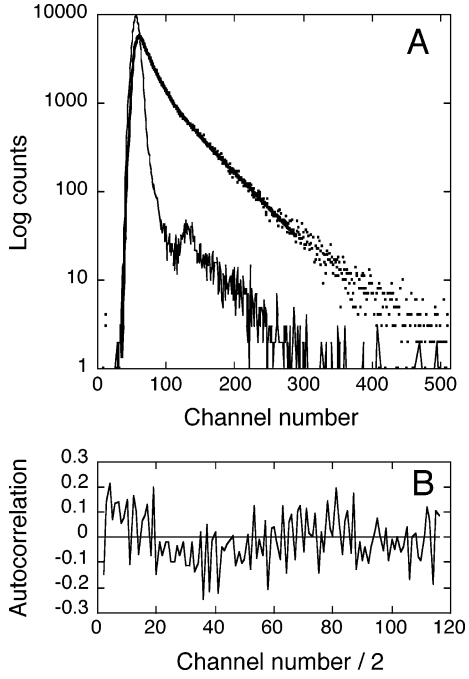

FIGURE 6: Time-resolved fluorescence intensity decay of *Bp*UreG under native conditions. (A) Typical fluorescence decay data, obtained at 24 °C using an excitation wavelength of 295 nm (slit width of 32 nm) and observing the fluorescence emission at 335 nm (slit width of 16 nm). The protein concentration was 0.2 mg/mL in 50 mM Tris-HCl buffer (pH 8.0) at 24 °C. The calibration time for each channel was 0.103 ns. On the *Y*-axis, the photon counts are reported in a logarithmic scale. The fast decaying, noisy solid line represents the impulse function (lamp) used as the excitation source. The slower decaying, noisy dotted line represents the experimental fluorescence decay curve, and with the smooth solid line is indicated the recovered fitting function. (B) Plot of the autocorrelation function of the weighted residual used to judge the goodness of the fitting.

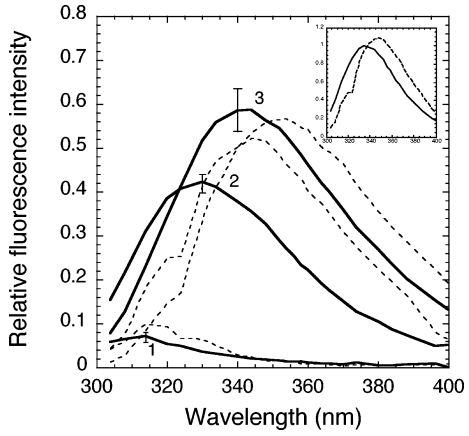

FIGURE 7: Decay-associated spectra (DAS) of *Bp*UreG under native and denaturing conditions. The solid lines represent the DAS obtained with *Bp*UreG (0.2 mg/mL in 50 mM Tris-HCl at pH 8.0 and 24 °C) under the native condition, whereas the dashed lines represent the DAS obtained with *Bp*UreG in the presence of 3 M GuHCl. Data were collected using an excitation wavelength of 295 nm. The DAS were obtained from the global analysis of multiple emission wavelength experiments (16−24 data sets). With 1, 2, and 3 are indicated the spectra (expressed as $\alpha_i\tau_i$ products) associated with τ_1, τ_2, and τ_3, respectively. Global reduced χ^2 values ranged from 1.05 to 1.38. In the inset, the sum of the relative DAS, obtained in the native and denatured states, is reported for comparison with the experimental steady-state spectra.

each decay component to the total emitted light of 4, 38, and 58%, respectively. On the other hand, in the presence of the denaturant, the spectra associated with $\tau_1-\tau_3$ were shifted to 315, 345, and 352 nm, respectively, and the relative contribution of each decay component to the total emitted light became 5, 44, and 51%, respectively.

The time-resolved results show that the increase in fluorescence induced by GuHCl on *Bp*UreG in the steady state takes place in the absence of significant effects on the decay constants, and the effect is mostly due to changes in the amplitudes. In particular, a predominant increase in the contribution of α_2 (DAS_2) is accompanied by a minor decrease in α_3 (DAS_3). In the inset of Figure 7, the overall change in the time-resolved spectral distribution of *Bp*UreG upon addiction of the denaturant is shown.

Changes in fluorescence intensity that involve solely changes in the decay amplitudes indicate the existence of a static mechanism. In general, this type of fluorescence quenching is observed when reactions in the ground-state generate nonradiative complexes. In proteins, static quenching of the intrinsic fluorescence may derive from charge transfer interactions between the tryptophan indole ring and the carbonyl or ammonium groups of the side chains of adjacent residues (*56*). Thus, our data for native *Bp*UreG are consistent with a structural organization that keeps the W192-containing loop relatively blocked, providing contacts between the indole ring and the side chains of the nearby residues. Upon addition of GuHCl, the spatial constraints of the W192-containing loop of *Bp*UreG in the native form are lost and the static quenching of W192 is released with an increase in fluorescence intensity.

Time-resolved fluorescence anisotropy has been used for a number of years to probe the rotational dynamics of globular proteins (*36*). Here, the anisotropy decay of the intrinsic fluorescence emission of residue W192 has been resolved to provide hydrodynamics information for *Bp*UreG at different denaturant concentrations. In the absence of denaturant, the fluorescence anisotropy transient reports on the hydrodynamic properties of *Bp*UreG in the native form, whereas at intermediate and high denaturant concentrations, the fluorescence anisotropy transient reports the hydrodynamic properties of *Bp*UreG in the more unfolded state. More explicitly, the recovery of a long correlation time, proportional to the volume and possibly to the shape of the hydrated protein, indicates the tumbling movements of the globular protein with native structure. On the other hand, the recovery of a short correlation time may indicate an increase in rotational dynamics due to the transition from the native to an unfolded state with disordered structure.

In Figure 8, an example of typical experimental data and results of analysis is presented. The time-resolved anisotropy parameters obtained in the different trials are reported in Table 3. Biexponential decays were found to describe appropriately the fluorescence anisotropy kinetics of *Bp*UreG under all tested conditions. The recovered sub-nanosecond correlation time (ϕ_1) is at the limit of our instrumental time resolution and can be reasonably assigned to the fast segmental motions of the tryptophan indole ring. On the other hand, the longer correlation time (ϕ_2) is consistent with the rotational Brownian motions of the protein as a whole. The long correlation time in the absence of GuHCl, 32.5 ns (see the footnotes of Table 3), corresponds to a Stokes radius of 31.2 Å (*36*). Despite the relative agreement with the value of 35 Å previously obtained using gel filtration methods (*33*),

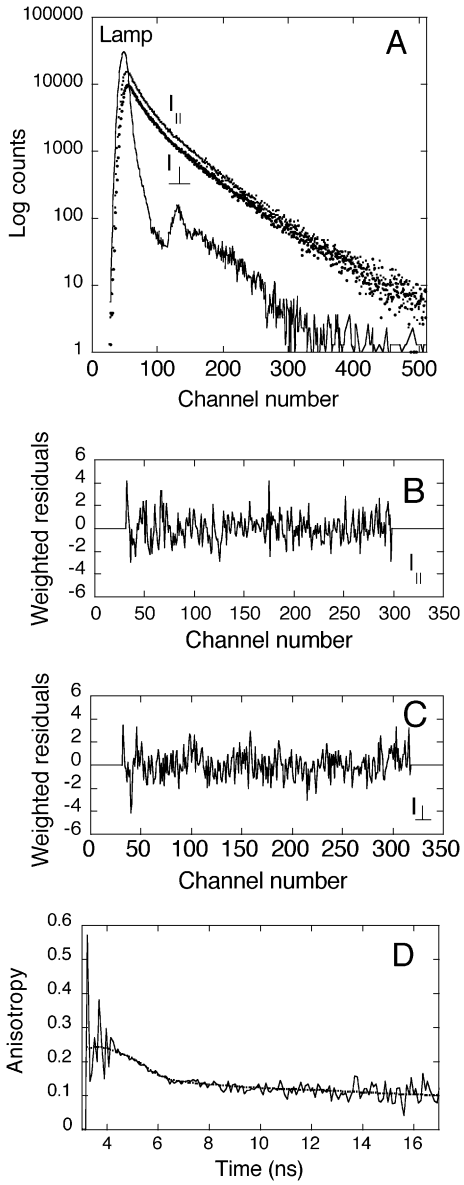

FIGURE 8: Anisotropy decay of *Bp*UreG. Fluorescence anisotropy decay of *Bp*UreG under native conditions [0.5 mg/mL in 50 mM Tris-HCl (pH 8.0)] at 24 °C. (A) With smaller and larger dots are reported the experimental decay components of the parallel ($I_{||}$) and perpendicular ($I_{\perp}$) polarized fluorescence, respectively. The solid line represents the impulse function (lamp) used as the excitation source. (B and C) Relative plots of the weighted residuals, commonly used to judge the quality of the fitting analysis. The graphs refer to the results of the analysis of the data obtained in the absence of GuHCl and presented in Table 3. (D) Convoluted time-resolved anisotropy.

the volume of this form of *Bp*UreG as measured by the Einstein−Stokes equation appears to be largely overestimated. In fact, considering the typical protein density of 1.35 g/mL and a hydration of 0.2 g of H_2O per gram of protein (*36*) and using a water dynamic viscosity of 0.911 cP at 24 °C, the expected correlation time for a protein of 46 kDa (i.e., the *Bp*UreG dimer) is 16 ns, and the corresponding hydrodynamic Stokes radius is 25.8 Å. The radius of 31.2 Å observed for *Bp*UreG can be explained either by a nonspherical symmetry of the protein or by an unusual content of water molecules bound to this form of the protein. This latter interpretation is more consistent with the partially unfolded nature of native *Bp*UreG (*33*). In the presence of 3.0 M GuHCl, at concentrations at which the induced conformational unfolding transition is mostly completed, the long correlation time is 10.6 ns. The observed decrease in the correlation time from 32.5 ns in the native state to 10.6 ns under denaturing conditions could be interpreted as being due either to a dimer-to-monomer conversion or to an increase in the rotational dynamics of the dimer caused by partial protein unfolding. The dissociation of the dimer is excluded by the light scattering data, as reported above, and therefore, these data are consistent with the rotational Brownian motions of a dimeric protein with some conserved structure (*36*).

Table 3: Time-Resolved Fluorescence Anisotropy Decay Parameters[a]

[GuHCl] (M)	β_1	ϕ_1 (ns)[b]	β_2	ϕ_2 (ns)	χ^2
0	0.14[c]	0.30[c]	0.13[c]	32.5[c]	1.27[c]
1.7	0.32[c]	0.13[c]	0.064[c]	11.7[c]	1.42[c]
3.0	0.17[c]	0.27[c]	0.051[c]	10.6[c]	1.04[c]

[a] In the table are reported the parameters recovered from the analysis of the experimental data presented in Figure 8. [b] The anisotropy decay curves were best fitted by two exponential anisotropy decay components. With ϕ_i values are indicated the correlation times and with β_i values their relative amplitudes. [c] Errors of the recovered parameters were estimated as the lower and upper bound of the joint confidence interval calculated for a 67% probability level (e.g., $\beta_1 = 0.09 < 0.14 < 0.17$, $\phi_1 = 0.17 < 0.30 < 0.46$ ns, $\beta_2 = 0.12 < 0.13 < 0.14$, and $\phi_2 = 21.2 < 32.5 < 51.9$ ns). Because of the highly unfavorable τ/ϕ ratio, the large error obtained for the upper bound of ϕ_2 recovered in the absence of denaturant is not representative of the errors obtained for the same parameter measured in the presence of 1.7 and 3.0 M GuHCl. In these cases, the typical error of ϕ_2 did not exceed 20% of the reported value.

DISCUSSION

In a previous report (*33*), Zambelli et al. have shown that *Bp*UreG, a protein involved in the urease active site assembly, features, in solution, a significant amount of secondary structure (15% α-helix and 29% β-strand) coexisting with a large conformational fluxionality of the protein backbone. In fact, the surprising peculiarity of *Bp*UreG and proteins of the same family, as evinced by NMR, CD, and light scattering studies, is the absence of a well-defined fold and rigid protein architecture (*33*). The lack of information about the actual form of the native state of *Bp*UreG, in particular with regard to which form of the Protein Quartet Model (*8*) (fully folded, molten globule, pre-molten globule, or random coil states) is assumed by the protein in solution, prompted us to carry out experiments based on fluorescence spectroscopy in the absence and presence of denaturant. In principle, this approach could reveal whether *Bp*UreG may be thought of being present in solution in any of these states and could monitor possible transitions between them. The analysis was performed by designing experiments that focused on the local environment of the main fluorophore W192 present in the protein, as well as experiments that are capable of monitoring the more global fold properties of the protein itself. For the first point, the model structure of *Bp*UreG derived using threading algorithms yielded a model of a very large fraction of the protein in the fully folded state (*33*) but did not provide any information about the C-terminal stretch that contains W192 (see Scheme 1), due to the lack of appropriate templates for the modeling

calculation. This portion of the protein was predicted to exist in an α-helical conformation (*33*), but it could not be determined whether this helix is adjacent to the main body of the protein or rather hanging out in a solvent-exposed environment. As for the global fold properties of the protein, experiments conducted using bis-ANS fluorescence were used to monitor the presence and evolution of hydrophobic regions of the protein that are exposed to the solvent in the native state and in the presence of denaturant. In addition, CD spectra were used to further investigate different aspects of the protein tertiary and secondary structure as a function of denaturant concentration.

The profile of the steady-state intrinsic fluorescence spectrum of the protein (Figure 1) recorded under native conditions, coupled with the bimolecular quenching rate constant ($k_q = 0.35 \times 10^9\ M^{-1}\ s^{-1}$) recovered by the measure of the intrinsic fluorescence quenching using KI (Figure 2A), indicates that indeed this residue is maintained in a solvent-protected environment. Overall, this evidence suggests that the C-terminal helix is packed against the body of the protein. On the other hand, the observation of a spectral red shift and the significant increase in the bimolecular quenching rate constant upon addition of denaturant (3 M GuHCl) reveal a higher polarity and a higher accessibility of the chemical environment of the indole ring of W192 to the solvent. In addition, the resolution in the nanosecond time scale of the decay-associated spectra (DAS in Figure 7) provides evidence that the 10% increase in the steady-state fluorescence intensity, observed in the presence of denaturant, can be explained by the release of a static quenching mechanism. Altogether, these results are consistent with a conformational transition affecting the architecture of the C-terminal helix, probed well by the intrinsic emission of W192. More specifically, it appears that in the native state the arm is lodged in the main core of the protein. Under these conditions, W192 is buried inside the protein matrix ("blue" spectrum, weak collisional quenching) and in close contact with the lateral groups of the neighbor residues (static quenching and lower emission intensity). In the state obtained by the addition of denaturant, the arm opens up and moves apart from the main core of the protein. Under these conditions, W192 is more exposed to the solvent ("red" spectrum, stronger collisional quenching) and far from close chemical interactions with the neighbor residues (release of the static quenching and higher emission intensity). Thus, we propose that the tryptophan-containing C-terminal peptide chain of *Bp*UreG can exhibit independent mobility from the main core of the protein. And yet, under proper biological requirements, this arm region may provide a relevant functional role.

Following this interpretation, the information that the motions of the C-terminal region are independent of a protein core that retains some structure is derived from the parameters of the equilibrium denaturation, measured by the changes in the steady-state intrinsic fluorescence intensity and anisotropy (Figure 3), a signal that probes uniquely the tryptophan residue contour. Indeed, a typical two-state transition is found with no evidence of observable intermediate states. The small $\Delta G^{\circ}_{0,un}$, the free energy change of unfolding extrapolated to zero denaturant concentration, determined for this transition, suggests that it involves a small rearrangement of the protein fold with the main body of *Bp*UreG still existing in a partially folded and structured state. The significant residual intrinsic steady-state anisotropy at 3 M GuHCl ($\langle r \rangle = 0.058$) strongly supports this view. In this respect, further evidence comes from the resolution of the anisotropy decay. Indeed, the long correlation time (ϕ_2) recovered under native conditions even in the presence of maximal denaturant concentrations (3 M GuHCl), likely assigned to the tumbling of a nonspherical and highly hydrated protein dimer, does not decline to the value expected for a fully unfolded protein. At 3 M GuHCl, ϕ_2 is fitted well by a time constant of 10.6 ns, a correlation time that definitely reports the rotational behavior of a structured protein's occupancy volume, rather than that of a protein in a random coil state. It is worth noticing that the excellent agreement between the steady-state anisotropies and the β_2 amplitudes measured at the corresponding denaturant concentrations (Figure 3B and Table 3, respectively) clearly indicates the reliability of the anisotropy decay data.

The results discussed so far rely on the intrinsic emission of residue W192, and they strictly report the nature and the changes of structural features affecting that particular chemical environment. Therefore, we have expanded our investigation on the global structure of *Bp*UreG by scanning the exposure of hydrophobic sites as a function of the denaturant concentrations, using bis-ANS as a fluorescent probe. Bis-ANS has been widely used to monitor hydrophobic patches at the protein surfaces (*57*) and to relate it to the formation of molten and pre-molten globule states (*58*). Proteins in the molten globule state exhibit a high affinity for hydrophobic fluorescence probes such as bis-ANS, because of the maximal exposure of the hydrophobic patches in this state. On the other hand, proteins in the pre-molten globule state display only residual interactions with hydrophobic probes, considerably weaker than in the molten globule, indicating that a minimal portion of the hydrophobic core, which is buried in the fully folded state but exposed in the molten globule state, is present in this protein form (*8*).

In our study, the high fluorescence intensity of bis-ANS in the native form (Figure 5A) reveals the presence of a large portion of exposed hydrophobic patches in the native form, which reach a maximal level of exposure at very low denaturant concentrations ([GuHCl] < 0.1 M). This behavior, atypical for a folded protein, can be explained in terms of a structure of *Bp*UreG that, in the native (N) form, is not fully folded but not yet in a molten globule state (see Figure 9). Supposedly, the potential interaction of *Bp*UreG with a partner protein (most likely the other urease chaperones UreD and UreF) may catalyze the conversion of the native disordered *Bp*UreG (N) into a native folded (F) "functional" form. From the N state, very small amounts of denaturant are sufficient to obtain a molten globule state (MG), characterized by maximal exposure of hydrophobic sites. This state still features large portions of secondary structure as shown by far-UV CD spectra (Figure 5B). From that state, as the denaturant concentration increases, a gradual decline in the fluorescence intensity of bis-ANS is observed that indicates a slow progressive disruption of the hydrophobic patches found exposed in the molten globule state. The secondary structure elements are largely conserved up to ca. 1.5 M GuHCl, as shown by far-UV CD (Figure 5B). At 3.0 M GuHCl, a large decrease in the ellipticity at 218 and 222 nm, typical for β and α secondary structure, is observed.

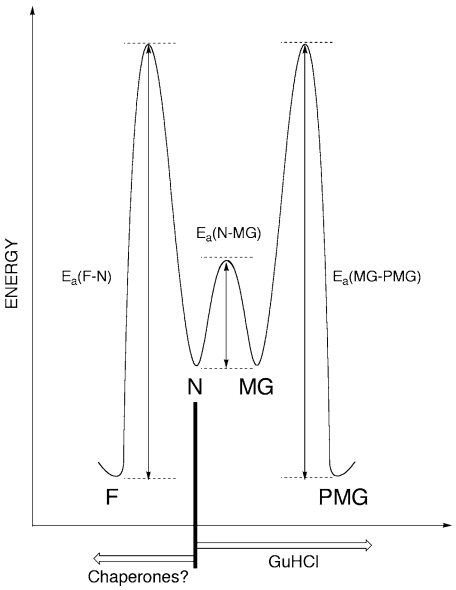

FIGURE 9: Proposed energy barrier model for *Bp*UreG structural transitions. Idealized energy profile for the folding states of *Bp*UreG as suggested by fluorescence spectroscopy. In the energy diagram, dimensions and shapes are reported arbitrarily. The states are as follows: F for the fully folded functional state, N for the native disordered state, MG for the molten globule state, and PMG for the pre-molten globule state. The arrows indicate the transitions observed by chemical denaturation or proposed to occur in the presence of partner chaperones.

The absence of positive ellipticity, typical for a random coil structure, indicates that some residual secondary structure is maintained, as typically found for a pre-molten globule state (PMG) (*8*). The absence of a fully random coil state at high denaturant concentrations, normally sufficient to completely unfold globular proteins, suggests that the pre-molten globule state of *Bp*UreG is a condition in which the protein is stable and more resistant to the complete denaturation with respect to a classical, well-behaved protein. The significant level of enzymatic GTPase activity detected for *Bp*UreG indicates that some fraction of UreG molecules in solution is correctly folded for catalysis or, alternatively, that the fold around the catalytic site is correct and the conformational fluxionality involves a different region of the protein (*33*). The presence of activity as well as the detection of secondary structure, in a protein without a rigid tertiary structure, is not surprising, considering that many IUPs have been shown not to be fully unfolded in solution but to contain portions of the sequence with an appreciable tendency to be preorganized or to possess a significant and often functionally related residual structure (*3*).

The analysis of the properties of *Bp*UreG in solution suggests that this protein belongs to the group of intrinsically unfolded proteins defined as denatured or disordered, rather than to the other group of IUPs defined as unstructured or unfolded (*2*, *8*). The presence of preformed structural elements may be useful in limiting the conformational search accompanying folding upon binding to the functional protein partners, a behavior found for many other IUPs (*3*). The existence of a disulfide bridge involved in the monomer subunit association in vitro, coupled with the previous knowledge (*33*) indicating that the dimeric species is significantly more folded than the monomer, suggests that a Cys−S−S−Cys bond could contribute in vivo to the assembly of a fully folded functional protein. The observed resilience of *Bp*UreG to fully unfold into a random coil state could be useful in facilitating the transition to the fully folded state (F) upon binding of UreG to the other partner proteins. It is worth mentioning that the fold of *Bp*UreG under native conditions is not affected by addition of Zn^{2+} or GTPγS, an analogue of GTP possessing much lower reactivity toward hydrolysis, as evidenced by $^{1}H-^{15}N$ HSQC NMR experiments (S. Ciurli and B. Zambelli, personal observations), and therefore, the interaction of this protein with UreD, UreF, and apourease must be essential for protein folding.

ACKNOWLEDGMENT

We thank Dott. Leonardo Gonnelli (from CERM) for assistance with the characterization of the protein using light scattering.

REFERENCES

1. Uversky, V. N. (2002) What does it mean to be natively unfolded? *Eur. J. Biochem. 269*, 2−12.
2. Fink, A. L. (2005) Natively unfolded proteins, *Curr. Opin. Struct. Biol. 15*, 35−41.
3. Tompa, P. (2005) The interplay between structure and function in intrinsically unstructured proteins, *FEBS Lett. 579*, 3346−3354.
4. Dyson, H. J., and Wright, P. E. (2005) Intrinsically unstructured proteins and their functions, *Nat. Rev. Mol. Cell Biol. 6*, 197−208.
5. Uversky, V. N., Oldfield, C. J., and Dunker, A. K. (2005) Showing your ID: Intrinsic disorder as an ID for recognition, regulation and cell signaling, *J. Mol. Recognit. 18*, 343−384.
6. Dunker, A. K., Brown, C. J., Lawson, J. D., Iakoucheva, L. M., and Obradovic, Z. (2002) Intrinsic disorder and protein function, *Biochemistry 41*, 6573−82.
7. Tompa, P. (2002) Intrinsically unstructured proteins, *Trends Biochem. Sci. 27*, 527−533.
8. Uversky, V. N. (2002) Natively unfolded proteins: A point where biology waits for physics, *Protein Sci. 11*, 739−756.
9. Tompa, P., and Csermely, P. (2004) The role of structural disorder in the function of RNA and protein chaperones, *FASEB J. 18*, 1169−1175.
10. Tompa, P., Szasz, C., and Buday, L. (2005) Structural disorder throws new light on moonlighting, *Trends Biochem. Sci. 30*, 484−489.
11. Hausinger, R. P. (1987) Nickel utilization by microorganisms, *Microbiol. Rev. 51*, 22−42.
12. Ciurli, S., and Mangani, S. (2001) in *Handbook on Metalloproteins* (Bertini, I., Sigel, A., and Sigel, H., Eds.) pp 669−708, Marcel Dekker, New York.
13. Hausinger, R. P., and Karplus, P. A. (2001) in *Handbook of Metalloproteins* (Messerschmidt, A., Huber, R., Poulos, T., and Wieghardt, K., Eds.) pp 867−879, John Wiley & Sons, Chichester, U.K.
14. Mobley, H. L. T., Island, M. D., and Hausinger, R. P. (1995) Molecular biology of microbial ureases, *Microbiol. Rev. 59*, 451−480.
15. Mulrooney, S. B., and Hausinger, R. P. (2003) Nickel uptake and utilization by microorganisms, *FEMS Microbiol. Rev. 27*, 239−261.
16. Lee, M. H., Mulrooney, S. B., and Hausinger, R. P. (1990) Purification, characterization, and in vivo reconstitution of *Klebsiella aerogenes* urease apoenzyme, *J. Bacteriol. 172*, 4427−4431.
17. Lee, M. Y., Pankratz, H. S., Wang, S., Scott, R. A., Finnegan, M. G., Johnson, M. K., Ippolito, J. A., Christianson, D. W., and Hausinger, R. P. (1993) Purification and characterization of *Klebsiella aerogenes* UreE protein: A nickel binding protein that functions in urease metallocenter assembly, *Protein Sci. 2*, 1042−1052.
18. Brayman, T. G., and Hausinger, R. P. (1996) Purification, characterization, and functional analysis of a truncated *Klebsiella aerogenes* UreE urease accessory protein lacking the histidine-rich carboxyl terminus, *J. Bacteriol. 178*, 5410−5416.
19. Colpas, G. J., Brayman, T. G., McCracken, J., Pressler, M. A., Babcock, G. T., Ming, L.-J., Colangelo, C. M., Scott, R. A., and

Hausinger, R. P. (1998) Spectroscopic characterization of metal binding by *Klebsiella aerogenes* UreE urease accessory protein, *J. Biol. Inorg. Chem. 3*, 150−160.
20. Colpas, G. J., Brayman, T. G., Ming, L. J., and Hausinger, R. P. (1999) Identification of metal-binding residues in the *Klebsiella aerogenes* urease nickel metallochaperone, UreE, *Biochemistry 38*, 4078−4088.
21. Colpas, G. J., and Hausinger, R. P. (2000) *In vivo* and *in vitro* kinetics of metal transfer by the *Klebsiella aerogenes* urease nickel metallochaperones, UreE*, *J. Biol. Chem. 275*, 10731−10737.
22. Remaut, H., Safarov, N., Ciurli, S., and Van Beeumen, J. J. (2001) Structural basis for Ni transport and assembly of the urease active site by the metallo-chaperone UreE from *Bacillus pasteurii*, *J. Biol. Chem. 276*, 49365−49370.
23. Song, H.-K., Mulrooney, S. B., Huber, R., and Hausinger, R. P. (2001) Crystal structure of *Klebsiella aerogenes* UreE, a nickel-binding metallochaperone for urease activation, *J. Biol. Chem. 276*, 49359−49364.
24. Park, I. S., Carr, M. B., and Hausinger, R. P. (1994) *In vitro* activation of urease apoprotein and role of UreD as a chaperone required for nickel metallocenter assembly, *Proc. Natl. Acad. Sci. U.S.A. 91*, 3233−3237.
25. Park, I. S., and Hausinger, R. P. (1995) Evidence for the presence of urease apoprotein complexes containing UreD, UreF, and UreG in cells that are competent for in vivo enzyme activation, *J. Bacteriol. 177*, 1947−1951.
26. Park, I. S., and Hausinger, R. P. (1995) Requirement of carbon dioxide for in vitro assembly of the urease nickel metallocenter, *Science 267*, 1156−1158.
27. Park, I.-S., and Hausinger, R. P. (1996) Metal ion interactions with urease and UreD-urease apoproteins, *Biochemistry 35*, 5345−5352.
28. Moncrief, M. C., and Hausinger, R. P. (1996) Purification and activation properties of UreD-UreF-urease apoprotein complexes, *J. Bacteriol. 178*, 5417−5421.
29. Heimer, S. R., and Mobley, H. L. (2001) Interaction of *Proteus mirabilis* urease apoenzyme and accessory proteins identified with yeast two-hybrid technology, *J. Bacteriol. 183*, 1423−1433.
30. Voland, P., Weeks, D. L., Marcus, E. A., Prinz, C., Sachs, G., and Scott, D. (2003) Interactions among the seven *Helicobacter pylori* proteins encoded by the urease gene cluster, *Am. J. Physiol. 284*, G96−G106.
31. Chang, Z., Kuchar, J., and Hausinger, R. P. (2004) Chemical cross-linking and mass spectrometric identification of sites of interaction for UreD, UreF, and urease, *J. Biol. Chem. 279*, 15305−15313.
32. Soriano, A., and Hausinger, R. P. (1999) GTP-dependent activation of urease apoprotein in complex with the UreD, UreF, and UreG accessory proteins, *Proc. Natl. Acad. Sci. U.S.A. 96*, 11140−11144.
33. Zambelli, B., Stola, M., Musiani, F., De Vriendt, K., Samyn, B., Devreese, B., Van Beeumen, J., Turano, P., Dikiy, A., Bryant, D. A., and Ciurli, S. (2005) UreG, a chaperone in the urease assembly process, is an intrinsically unstructured GTPase that specifically binds Zn^{2+}, *J. Biol. Chem. 280*, 4684−4695.
34. Moncrief, M. C., and Hausinger, R. P. (1997) Characterization of UreG, identification of a UreD-UreF-UreG complex, and evidence suggesting that a nucleotide-binding site in UreG is required for in vivo metallocenter assembly of *Klebsiella aerogenes* urease, *J. Bacteriol. 179*, 4081−4086.
35. Lehrer, S. S. (1971) Solute perturbation of protein fluorescence. The quenching of the tryptophyl fluorescence of model compounds and of lysozyme by iodide ion, *Biochemistry 10*, 3254−3263.
36. Lakowicz, J. R. (1999) *Principles of Fluorescence Spectroscopy*, Plenum Publishing, New York.
37. Chen, R. F., Knutson, J. R., Ziffer, H., and Porter, D. (1991) Fluorescence of tryptophan dipeptides: Correlations with the rotamer model, *Biochemistry 30*, 5184−5195.
38. Grinvald, A., and Steinberg, I. Z. (1974) On the analysis of fluorescence decay kinetics by the method of least-squares, *Anal. Biochem. 59*, 583−598.
39. Beechem, J. M., and Brand, L. (1985) Time-resolved fluorescence of proteins, *Annu. Rev. Biochem. 54*, 43−71.
40. Badea, M. G., and Brand, L. (1979) Time-resolved fluorescence measurements, *Methods Enzymol. 61*, 378−425.
41. Beechem, J. M., Gratton, E., Ameloot, M., Knutson, J. R., and Brand, L. (1991) in *Topics in Fluorescence Spectroscopy: Principles II* (Lakowicz, J. R., Ed.) Plenum Press, New York.
42. Bevington, P. R. (1969) *Data Reduction and Error Analysis for the Physical Sciences*, McGraw-Hill Inc., New York.
43. Pace, C. N. (1986) Determination and analysis of urea and guanidine hydrochloride denaturation curves, *Methods Enzymol. 131*, 266−280.
44. Eftink, M. R. (1994) The use of fluorescence methods to monitor unfolding transitions in proteins, *Biophys. J. 66*, 482−501.
45. Greenfield, N. J. (2004) Analysis of circular dichroism data, *Methods Enzymol. 383*, 282−317.
46. Jaenicke, R. (1999) Stability and folding of domain proteins, *Prog. Biophys. Mol. Biol. 71*, 155−241.
47. Schymkowitz, J. W., Rousseau, F., Irvine, L. R., and Itzhaki, L. S. (2000) The folding pathway of the cell-cycle regulatory protein p13suc1: Clues for the mechanism of domain swapping, *Struct. Folding Des. 8*, 89−100.
48. Simeoni, F., Masotti, L., and Neyroz, P. (2001) Structural role of the proline residues of the β-hinge region of p13suc1 as revealed by site-directed mutagenesis and fluorescence studies, *Biochemistry 40*, 8030−8042.
49. Wyatt, P. J. (1993) Light scattering and the absolute characterization of macromolecules, *Anal. Chim. Acta 272*, 1−40.
50. Wen, J., Arakawa, T., and Philo, J. S. (1996) Size-exclusion chromatography with on-line light scattering, absorbance, and refractive index detectors for studying proteins and their interactions, *Anal. Biochem. 240*, 155−166.
51. Habeeb, A. F. S. A. (1972) Reaction of protein sulfhydryl groups with Ellman's reagent, *Methods Enzymol. 25*, 457−464.
52. Bilsel, O., Yang, L., Zitzewitz, J. A., Beechem, J. M., and Matthews, C. R. (1999) Time-resolved fluorescence anisotropy study of the refolding reaction of the α-subunit of tryptophan synthase reveals nonmonotonic behavior of the rotational correlation time, *Biochemistry 38*, 4177−4187.
53. Musci, G., Metz, G. D., Tsunematsu, H., and Berliner, L. J. (1985) 4,4′-Bis[8-(phenylamino)naphthalene-1-sulfonate] binding to human thrombins: A sensitive exo site fluorescent affinity probe, *Biochemistry 24*, 2034−2039.
54. Semistonov, G. V., Rodionova, N. A., Razgulyaev, O. I., Uversky, V. N., Gripas, A. F., and Gilmanshin, R. I. (1991) Study of the molten globule intermediate state by a hydrophobic fluorescent probe, *Biopolymers 31*, 119−128.
55. Koshiba, T., Yao, M., Kobashigawa, Y., Demura, M., Nakagawa, A., Tanaka, I., Kuwajima, T., and Nitta, K. (2000) Structure and thermodynamics of the extraordinarily stable molten globule state of canine milk lysozyme, *Biochemistry 39*, 3248−3257.
56. Chang, M. C., Petrich, J. W., McDonald, D. B., and Fleming, G. R. (1983) Non-exponential fluorescence decay of tryptophan, tryptophylglycine, and glycyltryptophan, *J. Am. Chem. Soc. 105*, 3819−3824.
57. Smoot, A. L., Panda, M., Brazil, B. T., Buckle, A. M., Fersht, A. R., and Horowitz, P. M. (2001) The binding of *bis*-ANS to the isolated GroEL apical domain fragment induces the formation of a folding intermediate with increased hydrophobic surface not observed in tetradecameric GroEL, *Biochemistry 40*, 4484−4492.
58. Muzammil, S., Kumar, Y., and Tayyab, S. (1999) Molten globule-like state of human serum albumin at low pH, *Eur. J. Biochem. 266*, 26−32.
59. Morozova, L. A., Haynie, D. T., Arico-Muendel, C., Van Dael, H., and Dobson, C. M. (1995) Structural basis of the stability of a lysozyme molten globule, *Nat. Struct. Biol. 2*, 871−875.

BI060227S